Fon eca, J. *et al.* (2013). *Géotechnique* **63**, No. 6, 487 499 [h ://d .doi.o g/10.1680/geo 12.P.003]

Q an if ing he e ol ion of oil fab ic d ing hea ing ing di ec ional a ame

J. FONSECA*, C. O'SULLIVAN , M. R. COOP and P. D. LEE

O e he 50 ea , e e imen al die ha e e ea edl demon a ed ha he mechanical beha io of and i en i i e o he ma e ial fab ic, ha i , he a angemen of he g ain . U nil no he e ha e been ela i el fe a em o de c ibe hi fab ic an i a i el . M ch of o nde anding of he link be een he a icle mo emen and in e ac ion and he mac o- cale e on e of g an la ma e ial , incl ding and, come f om di c e e-elemen modelling and e imen on 'analog e' and i h im le, ideali ed ha e . Thi a e in e iga e me hod of an if ing he di ec ional fab ic of a eal and and i e ol ion nde loading. S a i ical anal e of he di ib ion of fab ic di ec ional da a in e m of a icle, con ac no mal, b anch ec o and oid o ien a ion e e ca ied o a diffe en age of hea ing defo ma ion. The da a ho ha he ini ial a icle o ien a ion fab ic ha de elo d ing he de o i ion of he ma e ial end o e i d ing hea ing, hile in he o - eak egime he con ac no mal eem o be eo ien ed along he di ec ion of he majo inci al e . Diffe en a e n e e ob e ed i hin he hea band, a boh he a icle and he con ac no mal ec o a ea ed o o a e along he hea lane.

KEYWORDS: fab ic/ c e of oil ; labo a o e ; mic o co and

INTRODUCTION

The e on e of oil and o he g an la ma e ial i kno n o be en i i e o he ma e ial fab ic, ha i , he o olog of he in e nal c e of he ma e ial. In geomechanic e- ea ch, fab ic ha been ali a i el de c ibed, and he fab ic change ha e f e en l been infe ed f om mac o- cale ob e a ion of oil e on e: fo e am le, ani o o of mall- ain iffne (e.g. K ano & Ja dine, 2002), ani o o of e meabili (e.g. Chan & Kenne , 1973), o com a i on of he mechanical e on e of ecimen e- a ed ing diffe en a oache (e.g. Vaid & Si a ha alan, 2000). Q an i a i e ob e a ion of fab ic ha e been made i h h ical model ing ho oela ic di c (e.g. Oda *et al.*, 1985) o Schneebeli od (e.g. Ib aim *et al.*, 2010), a ell a ing n me ical di c e e-elemen modelling (DEM) (e.g. Tho n on, 2000). Mo io mea emen of eal oil fab ic and he efe en ial o ien a ion of elemen of he oil fab ic ha e been ia ob e a ion of o-dimen ional image ing ei he o ical mic o co o canning elec on mic o- co (e.g. To e & Dade , 2002; Wilkin on, 2011). Fab ic can be an i ed ing ei he cala a ame e o di ec- ional a ame e . E am le of cala mea e of fab ic incl de he coo dina ion n mbe , he oid a io di ib ion i hin he am le, and he con ac inde . Di ec ional fab ic can be mea ed ing a icle long-a i o ien a ion o con ac no mal o ien a ion , and he a i ical a oache o anal e da a e of o ien a ion ec o a e ela i el ell e abli hed (Sa ake, 1982; Oda *et al.*, 1985; Tho n on, 2000).

E e imen al e idence of he effec of fab ic on he mechanical beha io of and ha been ho n b com a - ing he beha io of in ac and econ i ed am le (e.g. C e ell & Po ie, 2004; Ven o a & Coo , 2009). The e e e imen al die ha e demon a ed igni can diffe - ence in he eak eng h and dila ion fo boh ma e ial . The in ac ma e ial al o had a ma kedl highe iffne han he econ i ed and. The en i i of he mechanical e on e of and o fab ic can al o be ob e ed hen he mechanical e on e of econ i ed am le fo med ing diffe en e a a ion oced e a e com a ed (e.g. Been & Jeffe ie , 1985; Ib ahim & Kaga a, 1991). Oda (1972) and A h & Men ie (1972) e e among he o demon- a e he in ence of he ini ial fab ic o ien a ion on he eng h of and . E e imen al e idence of he effec of fab ic ani o o on oil iffne a e o ed b Zd a ko- ic & Ja dine (1997) (fo il) and K ano & Ja dine (2002) (fo and). All of he e mac o- cale da a e a e manife a ion of a a icle- cale ani o o ic e on e, and he ela ion hi be een he e o cale i con ide ed an i a i el he e.

The ke con ib ion of he c en o k be ond he e ea lie die i he e of mic o-com ed omog a h (mic o-CT) da a o gene a e h ee-dimen ional da a e fo eal oil gi ing a icle, con ac b anch ec o and oid o ien a ion . The da a e e obained a diffe en age d ing hea ing fo boh in ac and econ i ed am le , and o he allo f ndamen al ob e a ion of ma e ial e on e. Thi o k e end he ea lie con ib ion of Fon eca *et al.* (2012), ho con ide ed cala fab ic and a icle mo holog e ec i el . The a e gi e m- ma info ma ion on Reiga e and and he ia ial e e fo med. An o e ie of he me hod ed o an if di ec ional da a i gi en. Then he anal i and e l obained fo he fo da a e (he a icle , he con ac , he b anch ec o , and he oid) a e e en ed in n. Finall , he concl ion di c co ela ion be een he da a e , and con ide he e l in ela ion o bli hed DEM anal e .

Man c i ecei ed 3 Jan a 2012; e i ed man c i acce ed 28 Ma 2012. P bli hed online ahead of in 16 Oc obe 2012.
Di c ion on hi a e clo e on 1 Oc obe 2013, fo f he de ail ee . ii.

* Labo a oi e 3SR, Uni e i e Jo e h Fo ie , G enoble, F ance.
De a men of Ci il Enginee ing, Im e ial College London, UK.
De a men of Ci il and A chi ec al Enginee ing, Ci Uni e i , Hong Kong.
School of Ma e ial , The Uni e i of Manche e , UK.

SOIL DESCRIPTION AND TRIAXIAL TESTS

The sand investigated in this study is Reigate sand. This forms part of the Folkestone Beds formation (Lower Greensand), and the intact samples were retrieved from a quarry near Reigate (south-east England) where this geological formation outcrops. The material has a d_{50} of about 300 μm, and the grain geometries vary from being near-spherical to highly non-spherical. Fonseca *et al.* (2012) discuss the use of micro-CT and laser scanning data to quantify the particle morphologies for this material. Owing to the very high density and the interlocked fabric of the sand in its intact state, Reigate sand has been classified as a 'locked sand' meeting the criteria proposed by Dusseault & Morgenstern (1979). The sand provides an extreme example of fabric; in its intact state the grains are interlocked, and have no bonding between them. The reconstituted samples were obtained by tamping and vibration to densities close to those of the intact samples. The breakage of the fractured grains observed during reconstitution allowed the high densities to be attained even in the absence of interlocked grains; the reduction of the average mean particle diameter was of 13% (Fonseca *et al.*, 2012).

Thirteen triaxial tests were performed on a mixture of intact and reconstituted samples. Detailed test descriptions are given in Fonseca *et al.* (2012) and Fonseca (2011), and only a brief overview is provided here for clarity. All of the tests were carried out on dry samples that were isotropically consolidated to 300 kPa and then subjected to strain-controlled axial compression while keeping σ_3 constant. As has been documented in previous studies (e.g. Cuccovillo & Coop, 1999; Cresswell & Powrie, 2004), in comparison with the reconstituted and the intact material was stiffer, it attained a higher peak stress ratio, and it exhibited a higher rate of dilation. For both materials, equivalent tests were stopped at similar stages of the evolution of behaviour, but these corresponded to different axial strain levels. A single, well-defined shear plane was developed in both the intact and reconstituted samples. At the end of each test the sample was impregnated with an epoxy resin, and small cores were extracted for micro-CT. Four different shearing stages were thus considered: (1) prior to the start of compression; (2) at the onset of dilation; (3) the start of a visible shear band; and (4) as the sample approached a critical state. For stages 3 and 4 cores were taken both away from the developing shear band and across the shear band. The latter are identified with an 'S' in the sample reference in Table 1. The cores were larger than the shear band, which had an approximate thickness of $7d_{50}$ and $11d_{50}$ for the intact and reconstituted material respectively. Consequently the data from these cores cannot be representative of the soil within the shear band, and although care was taken to identify the shear band location, it is not possible to be exactly sure what proportion of the core samples was from inside and outside the shear band. As described elsewhere (e.g. Fonseca *et al.*, 2012) and summarised in Table 1, micro-CT scan data from eight intact and five reconstituted samples with a voxel size of 5 μm were reconstructed and processed to generate the data used in the current study to quantify the material anisotropy. The data were exported as three-dimensional arrays, where each voxel in the three-dimensional image was mapped to an array cell, and the analyses were then carried out using MATLAB (Mathworks, 2011).

Using a watershed segmentation (Beucher & Lantuejoul, 1979) implemented in an in-house code (Atwood *et al.*, 2004), each particle-phase voxel was assigned an integer identification number (id) to associate it with a specific grain. Contacts were identified along the boundaries of two regions of particle voxels by considering the voxel id numbers. Watershed segmentation was also used to identify individual voids.

QUANTIFYING DIRECTIONAL FABRIC

Figure 1 shows a schematic diagram of the fabric of an intact sample with an indication of the data considered in this study: the particle long-axis orientations (PO), the contact normal orientations (CN), the branch vector orientations (BV) and the void orientations (VO). Prior to presenting the data it is important to outline how the fabric was quantified. For each data set considered three approaches were used to quantify the fabric: two-dimensional rose diagrams, the distribution of contact orientations measured relative to the horizontal (angle ψ), and eigenvalue analysis of the three-dimensional fabric tensor.

Rose diagrams

A convenient way to plot the distribution of vector orientations is to use a rose diagram (i.e. an angular histogram). Where the vectors are three-dimensional these vector orientations can be plotted as a three-dimensional diagram; however, interpretation of this diagram is difficult. In the current study, for ease of visualisation, rose diagrams of the vector projections on the horizontal and vertical planes are presented. In the vertical plane the angle is measured relative to the horizontal, and in the horizontal

Table 1. Information on the samples investigated

Sample reference	Loading stage details			No. of particles		No. of voxels per particle (average)
	ε_a	q/p'	v	Total	Inner	
Int-1-a			1·48	2329	1438	74 059
Int-1-b			1·48	4078	2849	138 600
Int-2-a	0·37	1·96	1·46	3004	1930	55 936
Int-2-b	0·37	1·96	1·46	2633	1635	66 254
Int-3-a	3·89	1·73	1·63	3959	2574	40 513
Int-3-b-S	3·89	1·73	1·63	3082	1912	47 200
Int-4a	7·94	1·38	1·67	2618	1598	61 486
Int-4-b-S	7·94	1·38	1·67	5324	3247	104 570
Rec-1-a			1·50	3845	2513	39 893
Rec-1-b			1·50	3385	2110	169 740
Rec-3-a	9·66	1·46	1·87	4142	2704	35 977
Rec-3-b	9·66	1·46	1·87	4907	3387	27 504
Rec-4-S	12·35	1·46	1·70	3906	2591	35 070

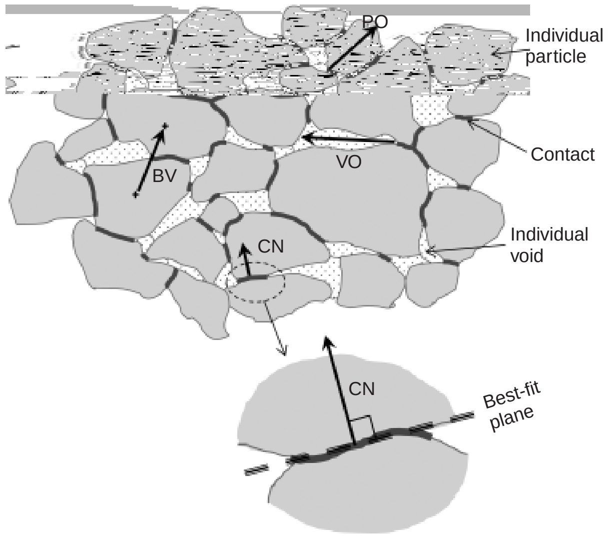

Fig. 1. Schematic diagram of fabric for intact sample, with indication of main features and vectors used for fabric quantification: particle orientation (PO), void orientation (VO), contact normal (CN) and branch vector (BV). Geometrical definition of CN vector included

lane is mea ed o a efe ence e ical lane. F he mo e, as he ec o da a e en ed he e a e o ien a ions i ho a s eci c di ec ion, onl one half of he lane need be cons id-e ed (i.e. in he x–y lane a ec o i h an o ien a ion of 330° o he osi i e x-a is is e i alen o a ec o i h an o ien a ion of 150° o he same a is). The da a se a ailable f om he mic o-CT scans allo ed co ela ions be een a i-cle, con ac and oid geome ies and o ien a ions o be made, and hese co ela ions e e e lo ed b shading he bins in he ose diag ams, fo e am le b a e age a icle si e.

Angle ψ inclination

In h ee dimens ions he o ien a ion of an ec o can be des c ibed in s he ical coo dina es as a combina ion of o angles: he a im h angle, gi ing he inclina ion of he ho i on al (x–y) ojec ion o he x-a is; and he angle ψ, hich, as ill s a ed in Fig. 2(a), is he angle be een he ec o and he ho i on al (x y) lane (i.e. he eni h angle is 90° − ψ). Fo a s mme ic o c oss-anis o o ic s am les, o ided he ma e ial is is o o ic in he ho i on al lane, he f e enc dis ib ion of he ψ angles fo a s ecimen gi es an indica ion of he fab ic anis o o . As ill s a ed in Fig. 2(a), his dis ib ion is de e mined b cons ide ing all he ni ec o s des c ibing he o ien a ions o o igina e a he cen e of a ni s he e. Then he n mbe of ec o s ha in e ce he s face of he s he e o e an ang la inc emen of dψ a e co n ed and no mali ed b he o al n mbe of ec o s. Fo an is o o ic ma e ial he f e enc dis ib ion is de e mined b cons ide ing inc emen al a ea dA (Fig. 2(a)) di ided b he o al s face a ea of he hemis he e. Ob-io s l , clos e o he a e of he s he e (fo ψ al es clos e o 90°) he a ea dA ass ocia ed i h he ang la inc emen dψ is m ch s malle han he dA al e ass ocia ed i h ψ al es clos e o 0°, and s o in he is o o ic cas e he es l an dis ib ion akes he non-linea fo m ill s a ed in Fig. 1(b). Fo he da a es en ed he e he ang la inc emen cons ide ed as 5°. In all cas es he e as s ca e in he e e imen al da a (o ing o he ni e n mbe of a icles and con ac s cons ide ed); cons e en l , fo each da a se cons ide ed, bo h he a da a and he s moo hed (l e ed) da a a e es en ed. The da a e e s moo hed i h he loess me hod a ailable in MATLAB (Ma h o ks , 2011), hich s es local eg ess ion i h eigh ed linea leas s a es and a s econd deg ee ol nomial.

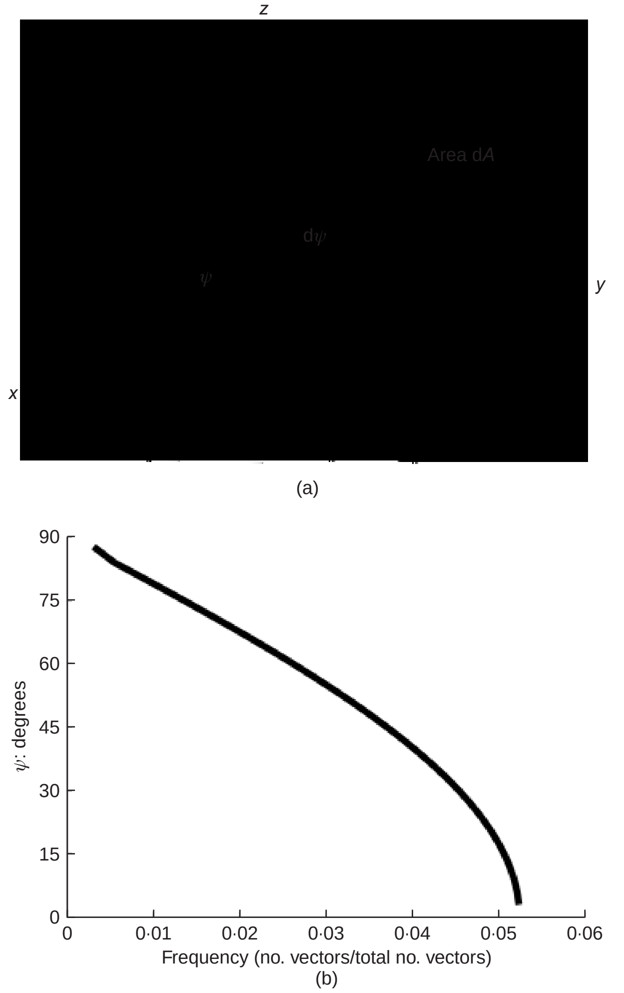

Fig. 2. (a) Definition of angle ψ, giving vector inclination to horizontal and illustration of discretisation of unit sphere to calculate distributions; (b) distribution of ψ values for isotropic case

Fabric tensor

The fab ic en so is commonl s ed o des c ibe he efe ed o ien a ion of a da a se of ec o s and is ass o-cia ed in en si . I akes gene al l he fo m of a s econd-o de s mme ic en so . Follo ing Sa ake (1982), he fab ic en so de ni ion s ed he e is

$$\Phi_{ij} = \frac{1}{N}\sum_{k=1}^{N} n_i^k n_j^k \qquad (3)$$

he e N is he o al n mbe of ec o s in he s s em and n_i^k is he ni o ien a ion ec o along di ec ion i. This de ni-ion of fab ic can be a lied o diffe en di ec ional ec o s des c ibing he s oil acking, incl ding he o ien a ion of he a icle majo a es (e.g. Dafalias *et al.*, 2004; Ng, 2004). Ho e e , his de ni ion does no acco n fo he s ha e of he a icles. A a icle hos e in e media e a is leng h is onl s ligh l bigge han is mino a is leng h o ld ha e he s ame con ib ion o he o e all en so as a a icle hos e in e media e a is leng h is j s s malle han is majo a is leng h. A fab ic en so ha cons ide s bo h a icle shape and particle orientation was introduced by Oda *et al.* (1985), and is given by

$$\Phi_{ij}^{a} = \frac{1}{\lambda}\sum_{k=1}^{N} T^{p}_{ki}T^{p}_{lj}S_{ij} \quad (4)$$

where N is the number of particles, and T_{ij} is the orientation tensor for particle p, which can be understood as follows. For a given point on the particle with coordinates x_i in a Cartesian coordinate system centred at the particle centroid, $x_j^{lp} = \boldsymbol{T}_{ij}x_i^{p}$ gives the coordinates of the same point with reference to a local coordinate system also centred on the particle centroid, but with axes aligned with the principal axes of inertia of the particle. The tensor S_{ij}^{p} is defined as

$$S_{ij}^{p} = \begin{bmatrix} a^{p} & 0 & 0 \\ 0 & b^{p} & 0 \\ 0 & 0 & c^{p} \end{bmatrix} \quad (5)$$

where a^p, b^p and c^p are the major, intermediate and minor half lengths of the particle, respectively. The index λ can be calculated by

$$\lambda = \sum_{p=1}^{N}(a^{p} + b^{p} + c^{p})$$

For each dataset considered, the sample anisotropy can be analysed by considering the difference between the maximum and minimum eigenvalues of the fabric tensor that is, $\Phi_1 - \Phi_3$. The orientation of the eigenvectors associated with the maximum eigenvalue gives an indication of the preferred fabric orientation.

PARTICLE ORIENTATIONS

The vectors describing the particles' major axis orientations were obtained by applying principal component analysis (PCA) to the cloud of points defining each grain. PCA is a mathematical tool that can be used to reduce the dimensionality (number of variables) of a dataset while retaining most of the original variability in the data, and the mathematics are outlined by Haralick & Shapiro (1992). This technique has been applied to tomographic data in other fields (e.g. Phillion *et al.*, 2008; Zhang *et al.*, 2009). Fonseca *et al.* (2012) used PCA when determining the particle aspect ratios. As the particles intersecting the boundary of the image were truncated, only the orientations of the inner, complete particles of the image were considered.

Figure 3 shows the rose diagrams of the projections of the particle long-axis orientation vectors onto the vertical (x–z) plane and horizontal (x–y) plane for representative intact and reconstituted samples prior to loading. As would be expected for this cross-anisotropic material, the projections onto the two orthogonal vertical y–z and x–z planes are equivalent and so only one vertical projection is presented here (i.e. the x–z plane). Each bin of the histogram is shaded according to the average elongation, as defined by the aspect ratio (ratio of minor axis length to major axis length) for the particles whose orientations are within that angular increment. Considering Fig. 3(a) (intact) and Fig. 3(c) (reconstituted), the distributions of the PO vectors for both samples types show a greater concentration around the horizontal plane: that is, perpendicular to the direction of deposition. This horizontal bias in the orientations is more marked for the intact soil. These data are reasonable, as when particles fall under gravity they tend to come to rest in their most stable positions: that is, their minor principal axes will be vertical (e.g. Cavarretta, 2009). Geological processes could cause post-depositional orientation changes for the intact material, but during sampling, site visits, no significant disturbance was observed in the soil strata, and there were no obvious depositional features such as cross-bedding. For the intact soil the more elongated particles, whose lower aspect ratios are represented by the lighter shading, are more likely to come to rest in this 'stable' position. The elongation bias is less marked in the reconstituted samples. The horizontal projections of both datasets do not indicate any particular directional bias; the small variations in the observed frequencies are a consequence of the finite number of PO vectors considered (Figs 3(b) and 3(d)).

The evolution of the particle orientations in the vertical plane during shearing can be appreciated by reference to Fig. 4, where rose diagrams for stage 3 (emergence of shear band) and stage 4 (close to the critical state) are presented. Referring to Fig. 4(a), outside the shear band in the intact material the particle orientations in the vertical plane become more isotropic, compared with Fig. 3(a); the same trend was observed for load stage 4. This is believed to be due to detachment of the small fragments, as the particles underwent breakage (Fonseca *et al.*, 2012), because these fragments would be more likely to have random orientations. This hypothesis is supported by the fact that in the reconstituted material the initial orientations are affected only by the appearance of the shear band. In comparison with the

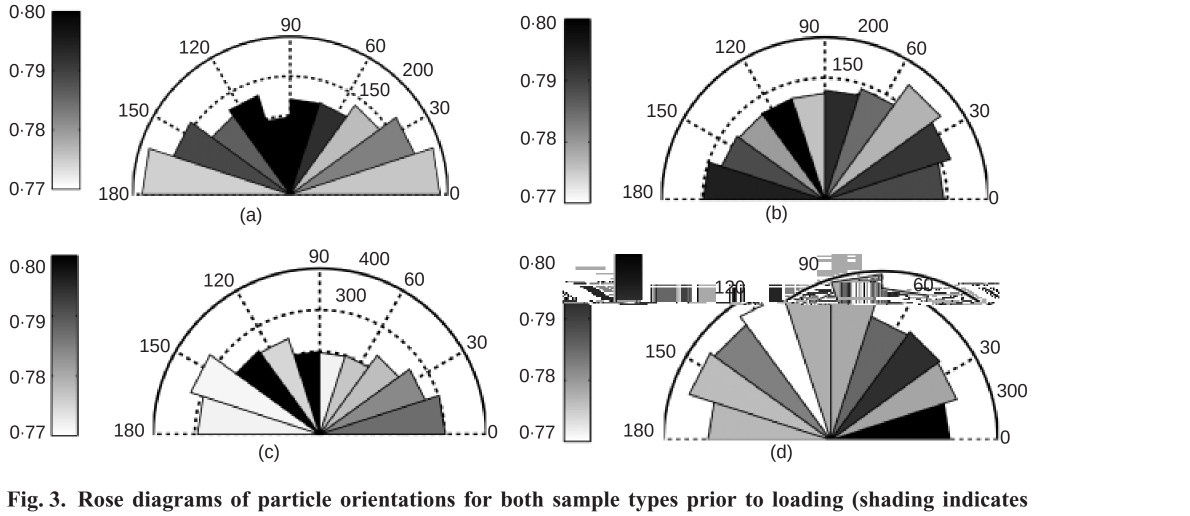

Fig. 3. Rose diagrams of particle orientations for both sample types prior to loading (shading indicates average aspect ratios of particles oriented within each angular bin): (a) vertical (x–z) plane Int-1-a; (b) horizontal (x–y) plane Int-1-a; (c) vertical (x–z) plane Rec-1-a; (d) horizontal (x–y) plane Rec-1-a

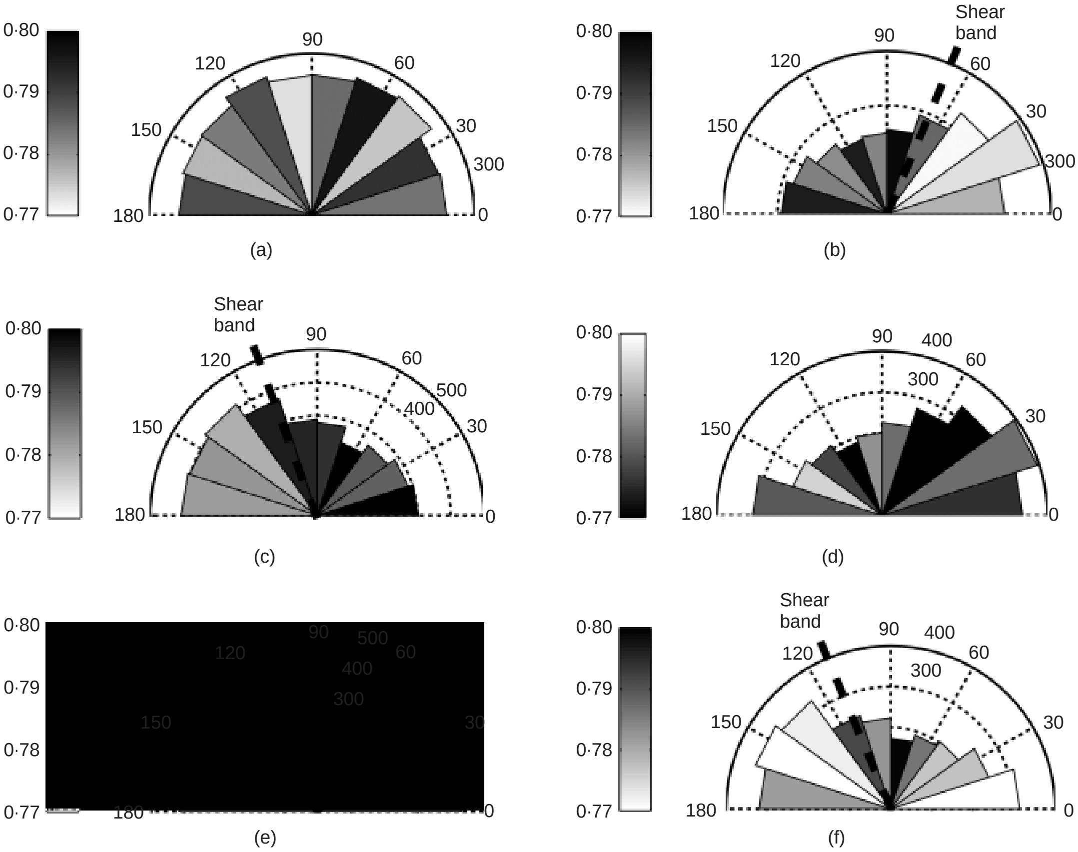

Fig. 4. Rose diagrams giving evolution of particle orientations during loading (shading indicates average aspect ratios of particles oriented within each angular bin): (a) vertical (x–z) plane Int-3-a; (b) vertical (x–z) plane Int-3-b-S; (c) vertical (x–z) plane Int-4-b-S; (d) vertical (y–z) plane Rec-3-a; (e) vertical (x–z) plane Rec-3-b; (f) vertical (x–z) plane Rec-4-S

initial condition, the particle orientations in the intact samples are no longer aspect-ratio dependent. While there is evidence that the particles fragmented along pre-existing cracks in the material, this process did not significantly change the range of aspect ratios in the material (Fonseca *et al.*, 2012). In both cases the particles in the samples that intersect the shear band (Figs 4(b), 4(c), 4(f) and to a lesser extent Figs 4(d) and 4(e)) reorientated during shearing, illustrating the heterogeneity of the sample response. As schematically illustrated in Fig. 5, the particles reorient in response to the shear band developing, an observation also reported by

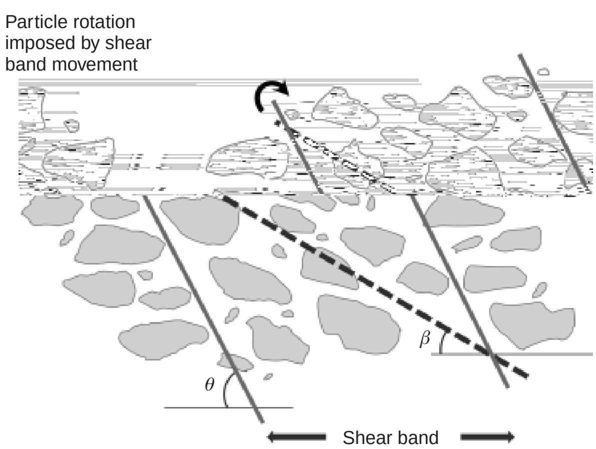

Fig. 5. Schematic diagram of change in fabric observed inside and outside shear band: angle *θ* indicates orientation of shear band; alignment of particles inside shear band given by angle *β* (major principal fabric)

Oda & Kazama (1998). The predominant particle orientation is given by the major principal fabric (angle β), and the orientation of the shear band is represented by θ.

The distributions of the ψ angles for the intact and reconstituted samples are illustrated in Fig. 6. Presenting the data in this format allows easy visualisation of the evolution of orientations. The smoothed data presented in Figs 6(b) and 6(d) confirm the trends observed in the rose diagrams. In comparison with an isotropic material, initially (stages 1 and 2) fewer particles are oriented with $\psi > 30°$, and more particles have closer to horizontal orientations (i.e. $\psi < 30°$) for both the intact and reconstituted soils. Outside the shear planes, the intact samples in stages 3 and 4 (Int-3-a and Int-4-a) have an almost isotropic distribution, with slightly fewer horizontally oriented particles (i.e. $\psi < 30°$) than in stages 1 and 2.

The deviatoric fabric data for the particles $\Phi_1^p - \Phi_3^p$ are given in Fig. 7, both considering the unweighted particle orientations and using the particle fabric tensor proposed by Oda *et al.* (1985). As was evident from the rose diagrams, the anisotropy of the intact material outside the shear band seems to decrease during loading. This evolution is not evident for the reconstituted material. Oda's fabric tensor indicates less significant differences in the anisotropy when comparing the material inside and outside the shear band. The orientation of the major principal fabric to the horizontal is illustrated in Fig. 8. The data confirm, to some extent, the earlier observations from Figs 3, 4 and 6: initially, with the exception of one data point, the orientations are less than 20° from the horizontal, indicating a strong preference towards horizontal orientations. As shearing progresses, the orientations become less clearly horizontal; however, the eigenvector orientations appear to be less effective than the

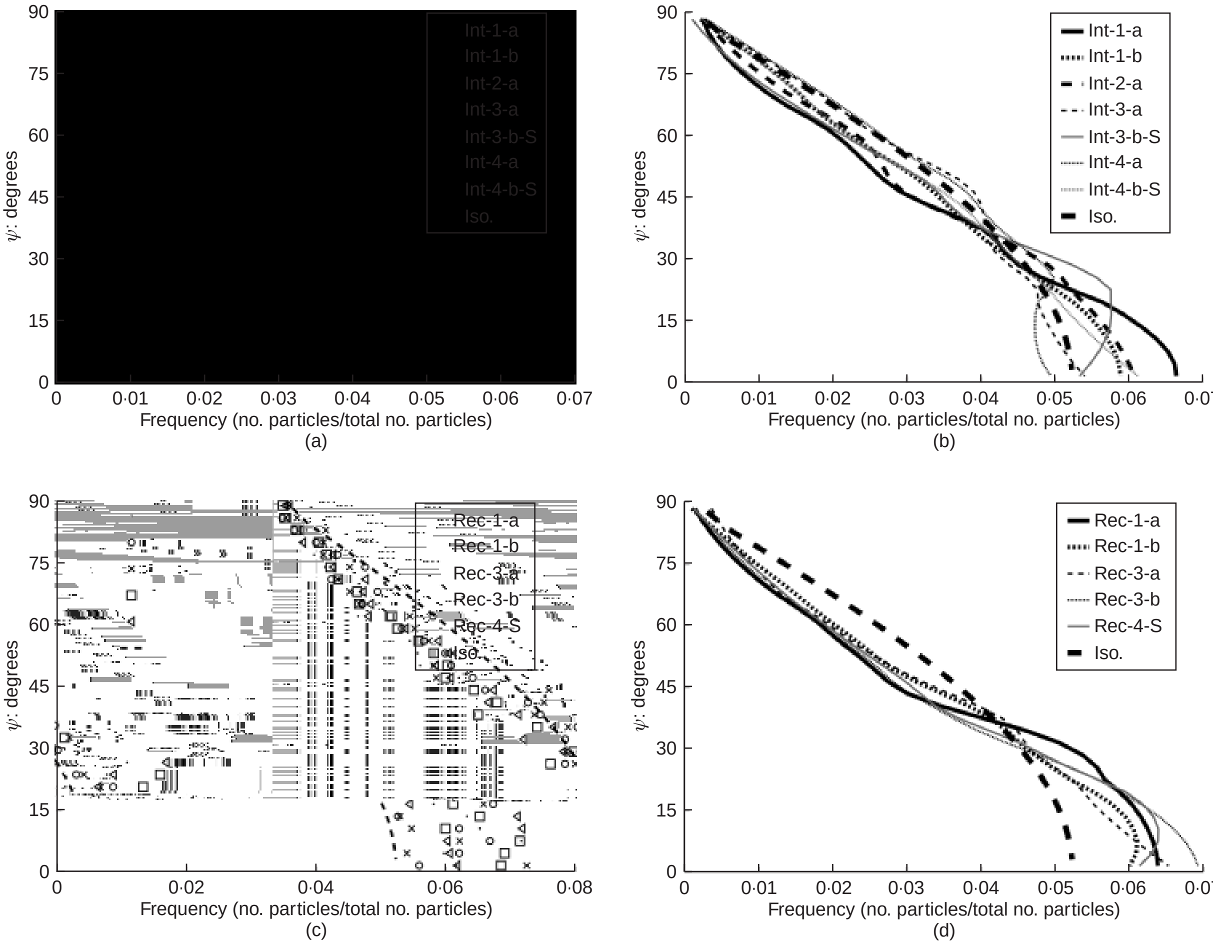

Fig. 6. Particle orientation (ψ angle) distribution for intact samples: (a) raw data for intact samples; (b) smoothed data for intact samples; (c) raw data for reconstituted samples; (d) smoothed data for reconstituted samples

o e diag am o f e en di ib ion in iden if ing a change in o ien a ion. Thi ma be beca e he ma e ial become lo ani o o ic a hea ing og e e .

The eigen ec o o ien a ion o ide in igh in o he ma e ial e on e i hin he hea band . The hea band o ien a ion a load age 4 e e 63° and 57° ela i e o he ho i on al fo he in ac and econ i ed ecimen e ec- i el . Table 2 gi e he o ien a ion of he majo inci al eigen ec o o he ho i on al (β^P) ing bo h he n- eigh ed and eigh ed a icle fab ic en o . The n- eigh ed fab ic en o gi e angle of 23° and 30° fo he in ac am le affec ed b he hea band a load age 3 and 4 e ec i el , and 20° fo he econ i ed am le a load age 4. The eigh ed fab ic en o add mo e eigh o he la ge a icle o gi e angle ha a e con ide abl lo e (5° o 9°); hi i an a e age al e, and he e l ill al o be inf enced b ho e a icle ha a e in he am le b no in he hea band. I i dif c l o ela e he e o ien a ion di ec l o he hea lane o ien a ion, o ing o he h ee-dimen ional na e of he hea lane, and nce - ain abo he e ac o ien a ion of he lind ical co e ela i e o hi lane. Thi ho ha fo bo h in ac and econ i ed am le he mall a icle ha e mo e andom o ien a ion , di e ging f om he main end.

CONTACT ORIENTATIONS

The o el e de ning each con ac fo med an i eg la face, o, a chema icall ill a ed in Fig. 1, a lea - a e eg e ion a a lied o iden if a be - lane fo each face, and hi lane de ned he con ac no mal o ien a ion. Fig 9 and 10 e en o e diag am of he con ac no mal o ien a ion io o hea ing and fo age 3 and 4. In Fig 9 and 10 each bin i haded b he a e age a ea of he con ac ho e no mal o ien a ion lie i hin ha bin. A he con ac a ea change igni can l d ing hea ing, a common g e cale ange canno be ado ed fo all he lo . The ho i on al ojec ion a e no ho n, a he e e i o o ic. Fig. 11 e en he di ib ion of con ac no mal o ien a ion o he ho i on al, and Fig 12 and 13 e en he ani o o and efe ed o ien a ion a calc la ed b eigen al e anal i of he fab ic en o . T o fab ic en o e e con ide ed: in he ca e, e a ion (3) a a lied di ec l ing he ni con ac no mal ec o , and in he econd ca e a eigh ed fab ic en o a calc - la ed a

$$\Phi_{ij}^{\mathrm{CN(W)}} = \frac{1}{\omega}\sum_{k=1}^{N} n_i^k n_j^k \omega^k \tag{6}$$

he e ω i he m of all he con ac i e , and ω^k i he i e of con ac k. Refe ing o Fig 9 and 11, io o loading he ec o ho e en iall an i o o ic di ib ion i h a ligh bia in he e ical di ec ion, fo bo h am le . The con ac a e igni can l malle fo he econ i ed am le. The e i al o a bia in he in ac am le fo he la ge con ac o ha e ho i on all o ien ed con ac no mal , and hi bia i no e iden fo he econ i ed ma e ial. Once hea ing commence , he e i a ed c ion in he con ac a ea fo he in ac am le . The e i al o a clea eo ien a ion of he efe en ial con ac no mal o ien a ion o a d he e ical (Fig 10, 11(b) and 11(d)), i h he

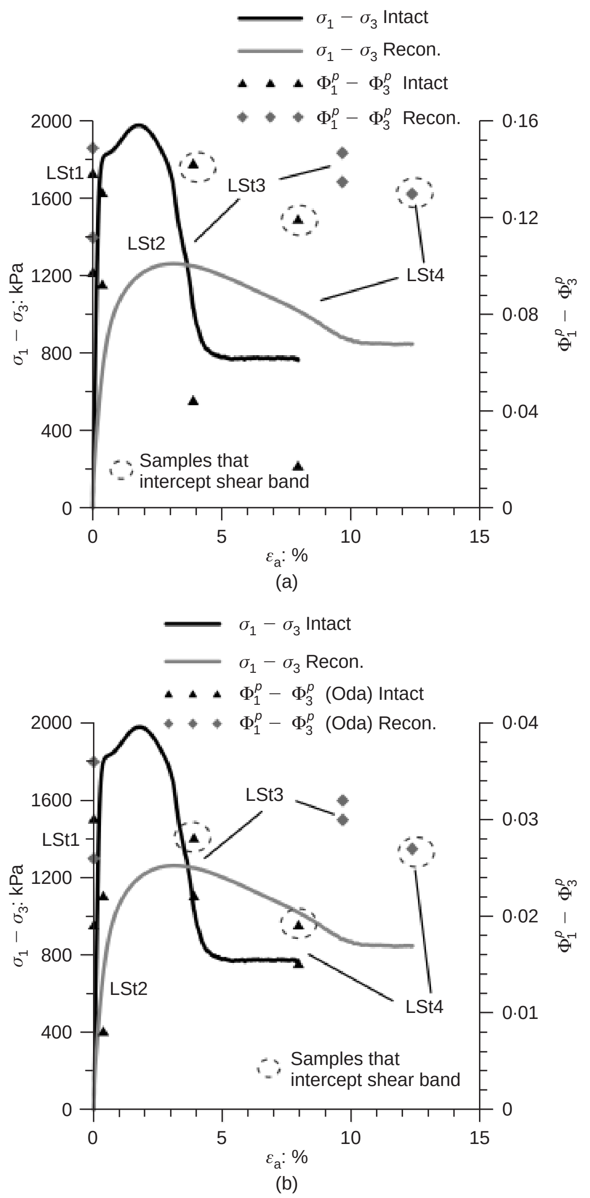

Fig. 7. Deviatoric fabric for particle orientations: (a) using 'simple' unweighted fabric tensor; (b) using fabric tensor for particle orientations proposed by Oda *et al.* (1985)

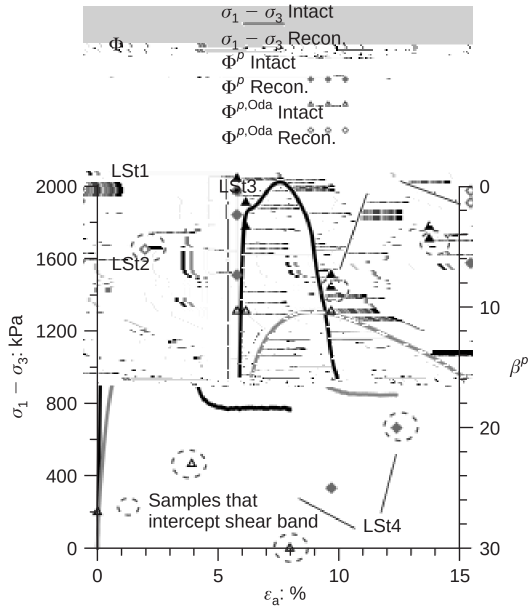

Fig. 8. Evolution of major principal fabric orientation using 'simple' unweighted fabric tensor for particle orientations, and fabric tensor for particle orientations proposed by Oda *et al.* (1985)

Table 2. Comparison of β values for unweighted (Φ^p) fabric tensor and using Oda *et al.* (1985) particle fabric tensor ($\Phi^{p,\mathrm{Oda}}$) for samples intercepting shear band

Sam le efe ence	β^p: deg ee	$\beta^{p,\mathrm{Oda}}$: deg ee
In-3-b-S	23	9
In-4-b-S	30	5
Rec-4-S	20	6

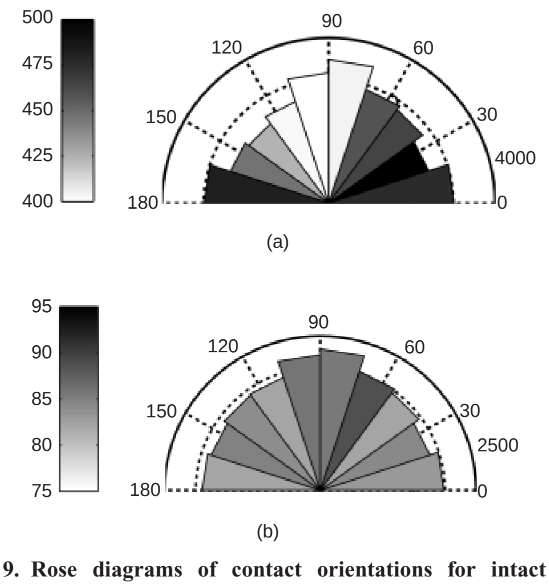

Fig. 9. Rose diagrams of contact orientations for intact and reconstituted samples prior to loading (shading indicates average contact area in μm² for contacts with normals oriented within each angular bin): (a) vertical (*x*–*z*) plane Int-1-b; (b) vertical (*x*–*z*) plane Rec-1-a

e en of hi eo ien a ion being imila fo bo h ma e ial , a e idenced in he inci al fab ic o ien a ion da a e- en ed in Fig. 13. Thi e of ealignmen of con ac no mal o be a o ima el coinciden i h he majo inci al e o ien a ion ha been demon a ed in n me - o DEM im la ion ing ideal a icle geome ie and con ac model (e.g. Ba e o, 2009). I gge he fo ma- ion of chain of a icle i h ela i el la ge, and hence able, con ac ha a e a allel o he majo inci al e di ec ion. The ela ion hi be een de ia o ic e ($\sigma_1 - \sigma_3$) and fab ic ($\Phi_1^{\mathrm{CN}} - \Phi_3^{\mathrm{CN}}$) e io l ob e ed in DEM im la ion (e.g. Tho n on, 2000) i le e iden . In a ic la , com a ing load age 1 and 2 in Fig. 12 he e i an ini ial dec ea e in ani o o ca ed b he de c ion of he inhe en fab ic on hea ing. Fo bo h he in ac and econ i ed ma e ial he al e of $\Phi_1^{\mathrm{CN}} - \Phi_3^{\mathrm{CN}}$ a e la ge in age 3 and 4 han in age 1 and 2, b i i no kno n hen hi inc ea e occ ed, o he he i a e- eak. Ho e e , he e i hen a clea o e all dec ea e in $\Phi_1^{\mathrm{CN}} - \Phi_3^{\mathrm{CN}}$ be een load age 3 and 4.

BRANCH VECTOR ORIENTATIONS

The b anch ec o i de ned a he ec o connec ing he cen oid of o a icle in con ac a ill a ed in Fig. 14. The o e diag am fo he ini ial b anch ec o a e

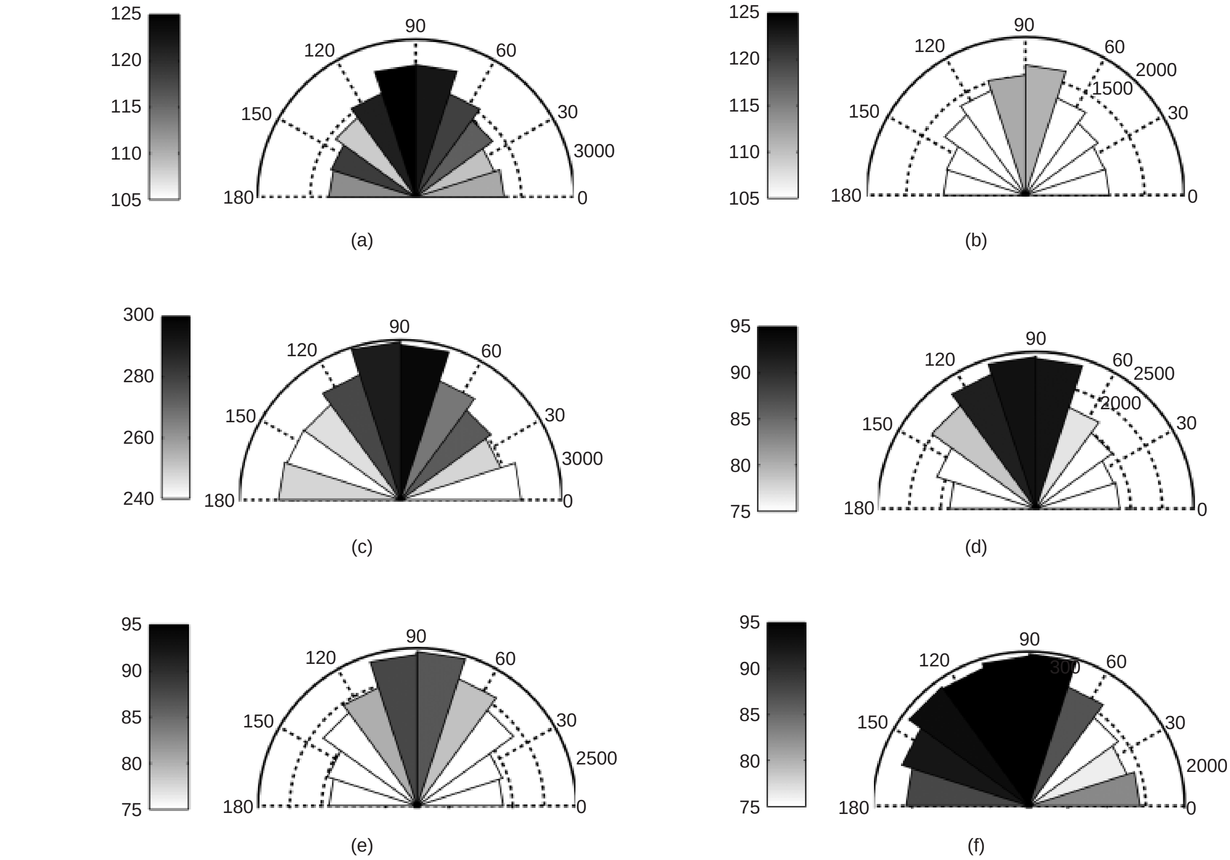

Fig. 10. Rose diagrams giving contact orientations for intact and reconstituted samples at stages 3 and 4 (shading indicates average contact area in μm² for contacts with normals oriented within each angular bin): (a) vertical (*x–z*) plane Int-3-a; (b) vertical (*x–z*) plane Int-3-b-S; (c) vertical (*x–z*) plane Int-4-b-S; (d) vertical (*x–z*) plane Rec-3-a; (e) vertical (*x–z*) plane Rec-3; (f) vertical (*x–z*) plane Rec-4-S

illustrated in Fig. 15, and as there was no apparent bias in the orientations with branch vector lengths, shading has been omitted for clarity. In comparison with the contact normal orientations, the vectors have a more isotropic distribution in the vertical plane. The eigenvector orientations during shearing are shown in Fig. 16, and it is clear for the intact samples that, as shearing progresses, the branch vectors are more likely to have a vertical orientation, excluding the samples that partially intersect the shear band; this tendency is less evident for the reconstituted samples. As was the case with the deviatoric fabric $\Phi_1^{CN} - \Phi_3^{CN}$ it is difficult to assess, in Fig. 17 whether $\Phi_1^{BV} - \Phi_3^{BV}$ increases between the initial and peak stages, but there does appear to be a decrease in $\Phi_1^{BV} - \Phi_3^{BV}$ between loading stages 3 and 4.

It does not necessarily follow that the branch vectors and the contact vectors should be collinear, and referring to the schematic diagram in Fig. 14, where these vectors are not collinear, there is a moment transmission at the contacts (e.g. O'Sullivan, 2011). The relationship between the branch vectors and the contact normals was investigated by considering the angle between the two vectors, denoted by α. The distribution of α is plotted in Fig. 18 for the intact samples outside the shear band (Int-1-a, Int-2-a, Int-3-a and Int-4-a). With the exception of a few cases the maximum value of α is 60°, and the most frequent value of α is approximately 20°. No significant variation can be seen for samples at different load stages, which is in agreement with the observation made by Ng (1999), although Ng did report a significantly narrower range of α values. For the current study α tended to decrease with increasing contact size.

VOID ORIENTATIONS

While particles are physical features in the image, the definition of individual voids is more abstract or subjective, as voids connect with each other (Shire *et al.*, 2012). As noted above, here a watershed segmentation approach was used to distinguish individual pores (Atwood *et al.*, 2004). The void analysis was carried out for six samples at load stages 1 and 3. Given the smaller amount of void data, the eigenvalue analysis data are not considered here. Fig. 19 illustrates the initial void orientations, and these seem to have a slight bias towards being horizontally oriented, particularly for the reconstituted sample. However, during shearing this bias is eliminated, with the voids seeming to be slightly vertically oriented (Fig. 20). The shear band clearly influences the overall distribution of void orientations, as evidenced in Fig. 20(b).

DISCUSSION

The analyses of the micro-CT data, including the particle morphologies (Fonseca *et al.*, 2012), the scalar data on soil fabric and the directional fabric data presented here, allow a conceptual model of the soil response to be created, as summarised in the schematic diagrams in Fig. 21. Fig. 21(a) shows the intact soil prior to loading; the majority of the particles are horizontally oriented, and a similar trend is observed for the voids. Both the contact normal vectors and the branch vectors show a more isotropic distribution. For the intact soil in the post-peak regime, the large particles are essentially horizontal, while the detached fragments

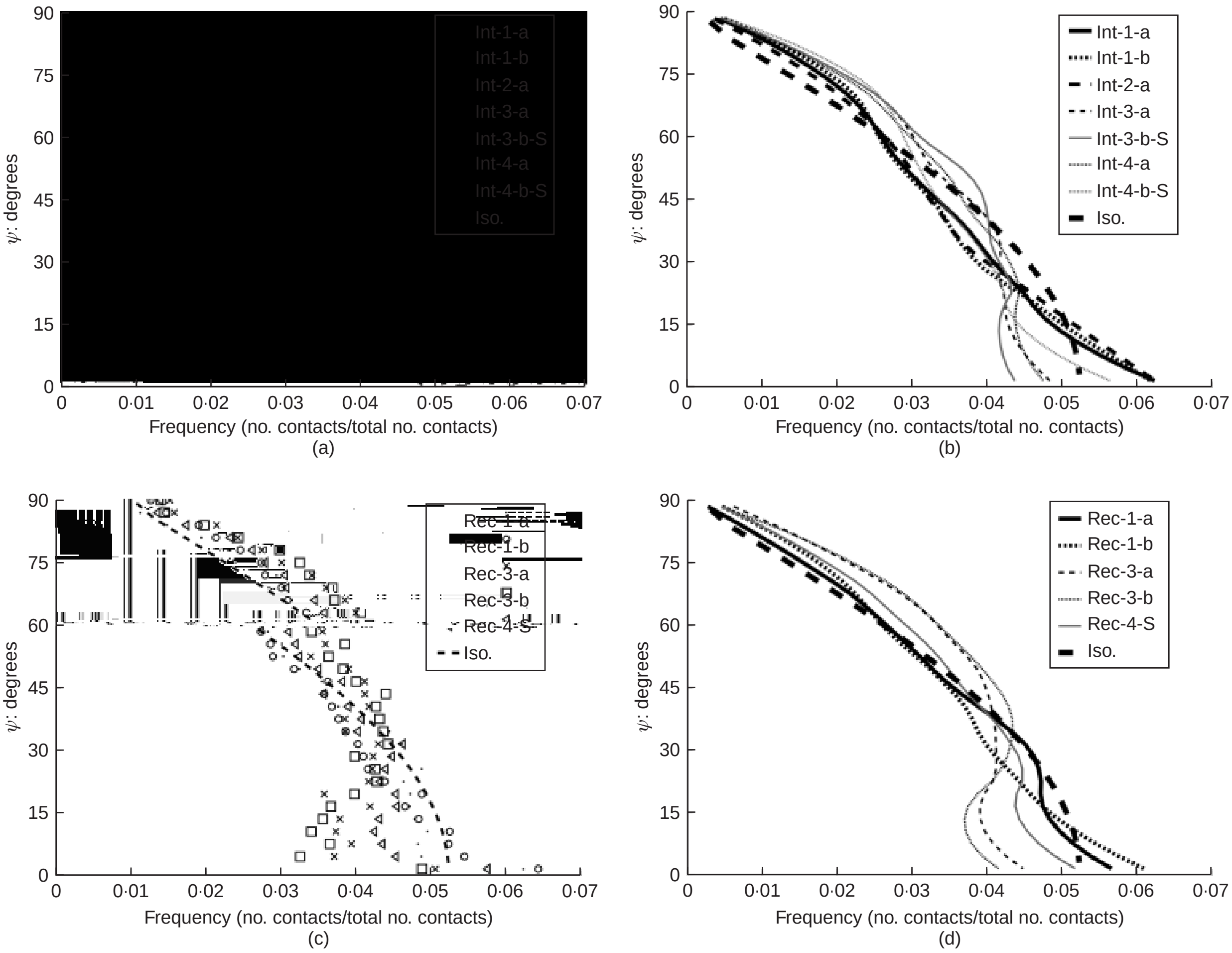

Fig. 11. Contact normal orientation (ϕ angle) distributions for intact samples: (a) raw data for intact samples; (b) smoothed data for intact samples; (c) raw data for reconstituted samples; (d) smoothed data for reconstituted samples

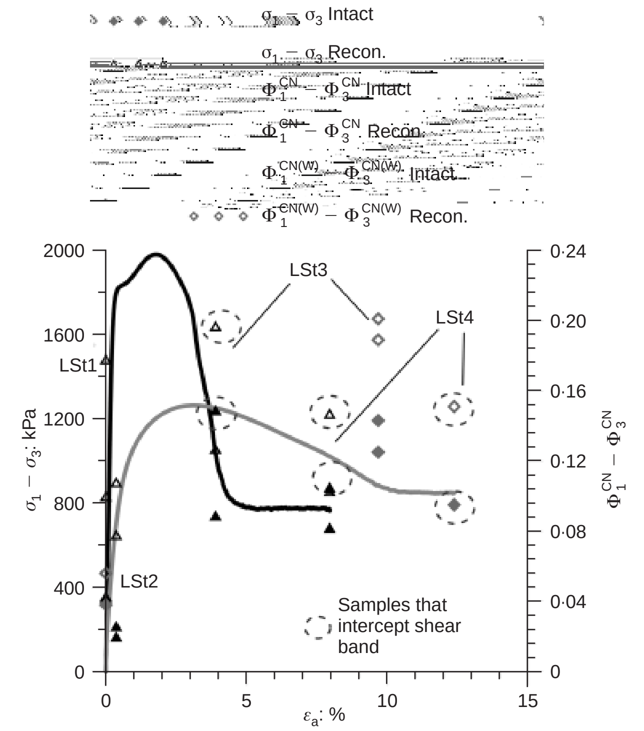

Fig. 12. Contact normal deviatoric fabric evolution during loading

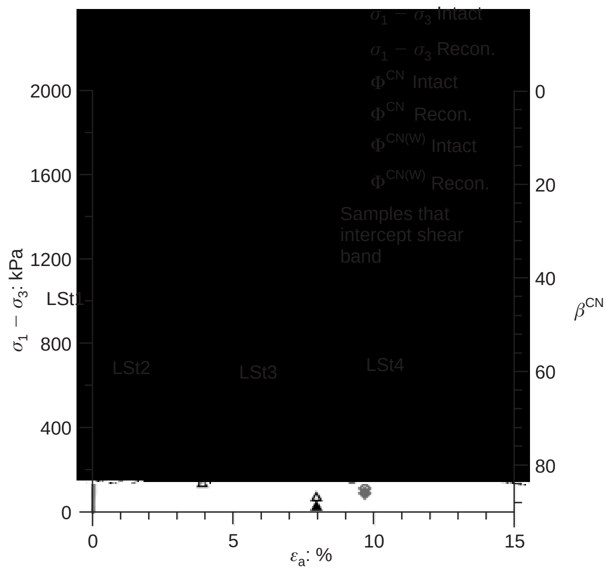

Fig. 13. Evolution of major principal fabric orientation for contact normals using unweighted fabric tensor for particle orientations, and weighted fabric tensor for particle orientations

e hibi andom o ien a ion (Fig. 21(b)). A hi age he oid ho an inc ea e in i e a co e ence of he dila ion, and hei o ien a ion a e mo e andom com a ed i h he e io age. O ide he hea band he con ac

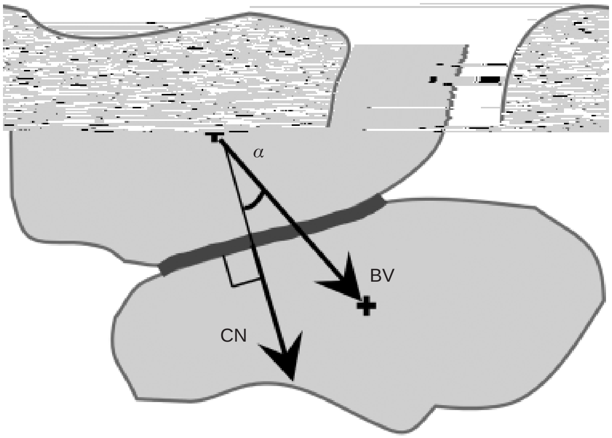

Fig. 14. Schematic diagram illustrating branch vector and contact normal

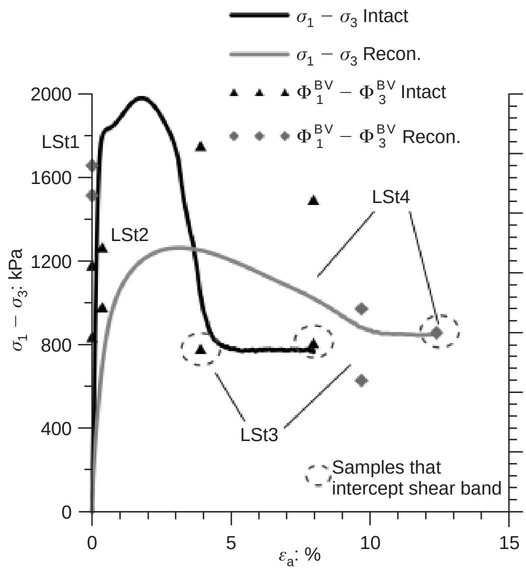

Fig. 16. Evolution of deviatoric fabric for branch vectors

no mal ha e a ong concen a ion along he e ical, and he b anch ec o ho a ligh concen a ion, al o along he e ical di ec ion. Fo he ame age, he mo emen along he hea band ca e he a icle o o a e in he di ec ion of he hea lane (Fig. 21(c)). The efo e, in ide he hea band, he con ac no mal ec o and he b anch ec o ho a de ia ion f om he e ical lane o a d he di ec ion of he hea lane.

Fo he econ i ed oil io o loading, a iden i ed b Fon eca *et al.* (2012), he mall f agmen ha e been de ached f om he la ge a icle d ing econ i ion, e en if he econ i ion occ a ca ied o e gen l . The majo i of he a icle , ega dle of hei i e, ho a ho i on al o ien a ion (Fig. 21(d)). The di ib ion of he b anch ec o and he oid ho a ligh concen a ion along he ho i on al di ec ion, hile he con ac no mal e hibi an i o o ic di ib ion. In he o eak egime he a icle emain e en iall ho i on al o ide he hea band, hile he con ac no mal ho a ong concen a ion along he e ical di ec ion, and a imila e le ono nced end i ob e ed fo he b anch ec o (Fig. 21(e)). A he ame age, he mo emen ca ed b he hea band make he a icle o a e o a d he di ec ion of he hea lane, and he con ac no mal and b anch ec o al o end o de ia e f om he e ical di ec ion in ide he hea band (Fig. 21(f)).

CONCLUSIONS

Mic o-CT a ed o e end o nde anding of oil e on e a he a icle cale b di ec l and an i a i el anal ing he di ec ional fab ic of in ac and econ i ed oil in h ee dimen ion a a io oin d ing hea ing.

(*a*) In hei ini ial a e he a icle long-a i o ien a ion ended o be o ien ed in he ho i on al lane, ha i , e endic la o he di ec ion of de o i ion.

(*b*) Fo he econ i ed am le , he ini ial ho i on al efe ed o ien a ion a i ed e en af e a c i ical a e had a a en l been eached (fo he a icle no affec ed b he hea band mo emen).

(*c*) Fo he in ac oil, he mall f agmen de ached d ing he dila ion of he oil e hibi andom o ien a ion , b he la ge g ain emain e en iall ho i on al. A a icle

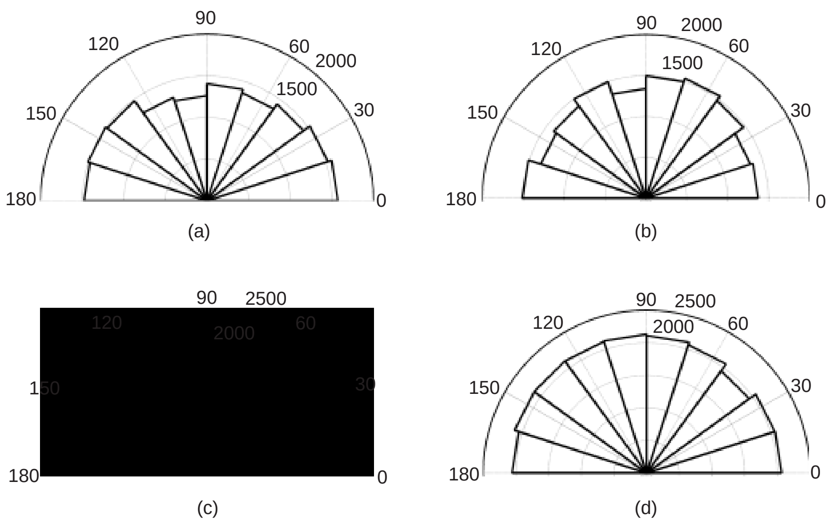

[redacted]

Fig. 15. Branch vector orientations for both sample types prior to loading: (a) vertical (x–z) plane Int-1-a; (b) horizontal (x–y) plane Int-1-a; (c) vertical (x–z) plane Rec-1-a; (d) horizontal (x–y) plane Rec-1-a

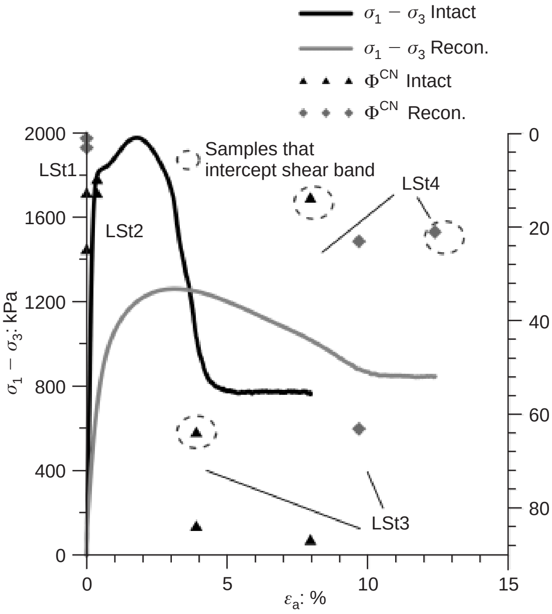

Fig. 17. Evolution of major principal fabric orientation for branch vectors

o ien a ion fab ic en o ha ake in o con ide a ion he i e and ha e of he g ain i be e o de c ibe he fab ic e ol ion of hi ma e ial on hea ing.

(*d*) The concen a ion of con ac no mal along he di ec ion of he majo inci al e a ob e ed in he o - eak egime fo bo h he in ac and econ i ed oil, a o la ed b he fo ce chain heo and ob e ed in io ho oela ic e and DEM anal e . The effec of he mo emen in ide he hea band a o de ia e he con ac no mal ec o f om he e ical, hich i a ocia ed i h he b ckling of he fo ce chain . In con a o he e on e ob e ed in ho oela ic and DEM anal e , on hea ing, fo bo h ma e ial , he con ac no mal de ia o ic fab ic e hibi an ini ial dec ea e, indica ing a de c ing of he ma e ial.

(*e*) The b anch ec o o ien a ion al o became mo e e ical d ing hea ing, b he end a light diffe en in ho a am le ha in e ce ed he hea band. The b anch ec o and con ac no mal ended no o be collinea , i h he angle f e en diffe ing b 20°.

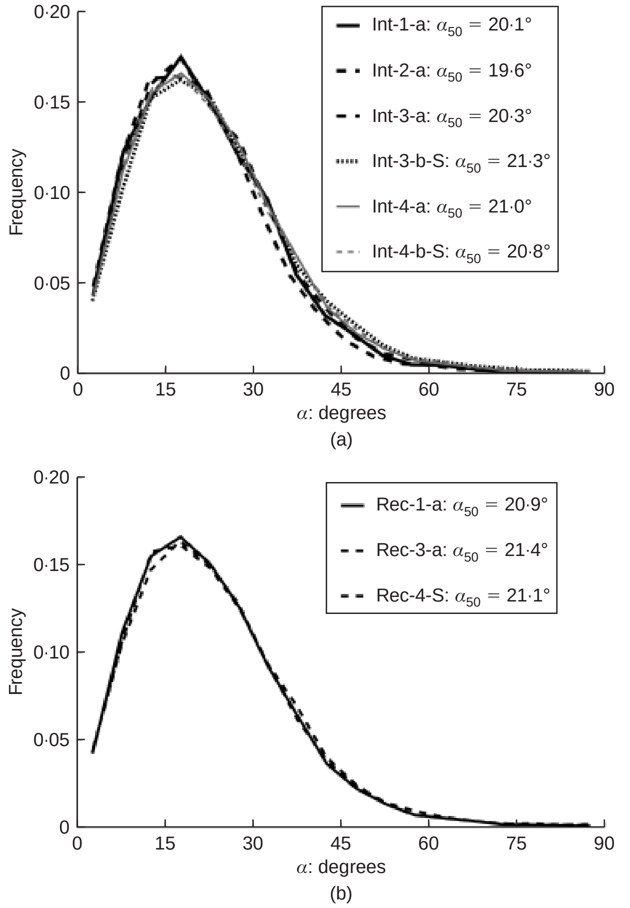

Fig. 18. Distribution of angle α between branch vectors and contact normals, indicating median values (i.e. α_{50}): (a) intact samples; (b) reconstituted samples

(*f*) Ini iall he oid ended o ha e a ligh ho i on al bia in hei long-a i o ien a ion , j a he ca e fo he a icle , b on hea ing hi bia became le e iden

ACKNOWLEDGEMENTS

The in e iga ion e en ed in hi a e a ca ied o nde he nancial o of a Po g e e go e nmen

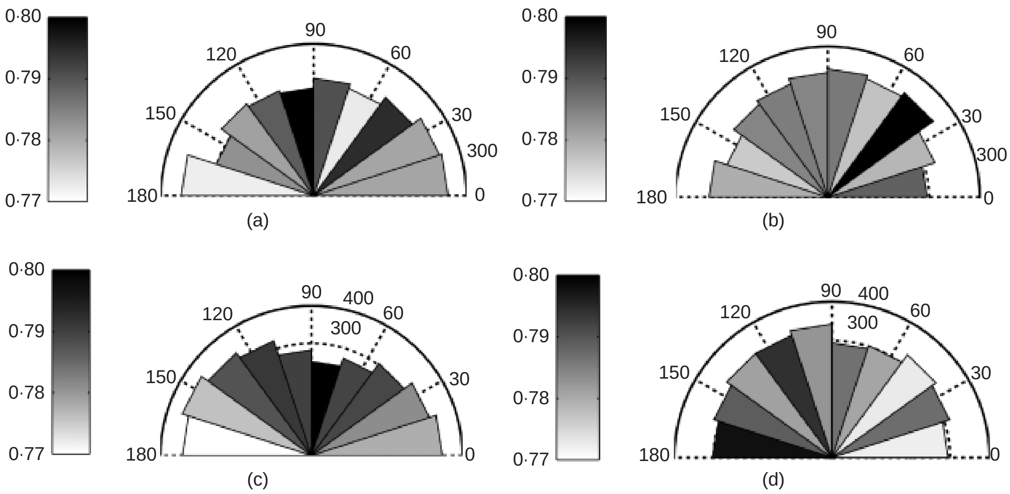

Fig. 19. Void long-axis orientations for both intact and reconstituted samples prior to loading (shading indicates average void volume in μm³ for voids with long axes oriented within each angular bin): (a) vertical (x–z) plane Int-1-a; (b) horizontal (x–y) plane Int-1-a; (c) vertical (x–z) plane Rec-1-a; (d) horizontal (x–y) plane Rec-1-a

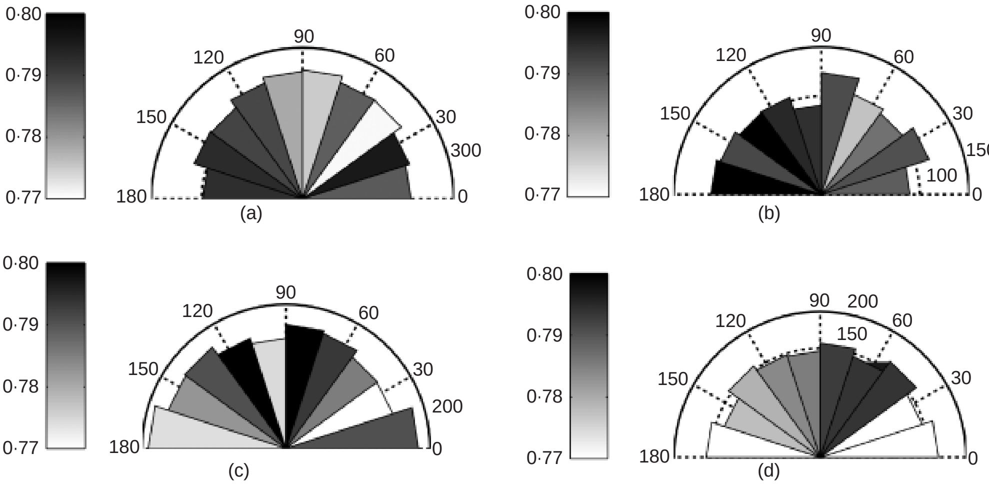

Fig. 20. Void long-axis orientations for intact and reconstituted samples, illustration of evolution during loading (shading indicates average void volume in μm^3 for voids with long axes oriented within each angular bin): (a) vertical (x–z) plane Int-3-a; (b) vertical (x–z) plane Int-3-b-S; (c) vertical (x–z) plane Rec-3-a; (d) vertical (x–z) plane Rec-3-b

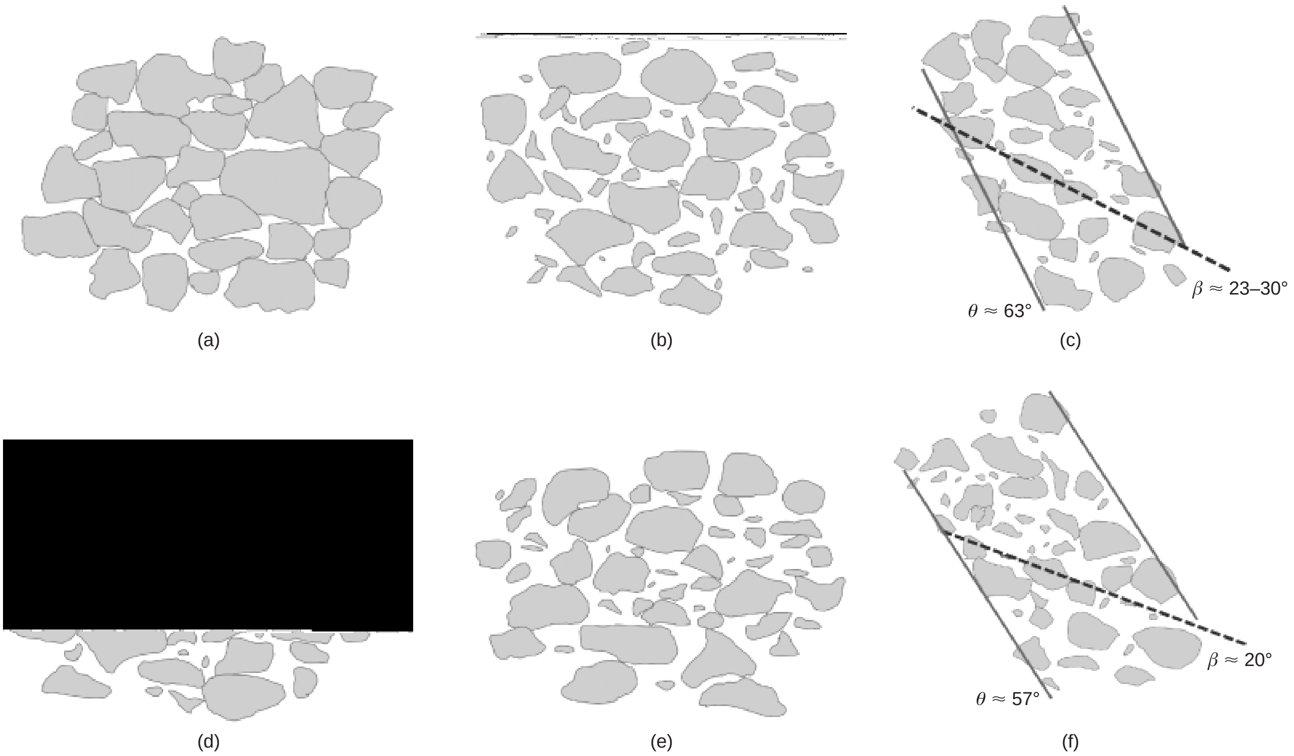

Fig. 21. Schematic diagrams of soil fabric at different stages of loading: (a) intact soil prior to loading; (b) intact soil in post-peak regime outside shear band; (c) intact soil in post-peak regime inside shear band; (d) reconstituted soil prior to loading; (e) reconstituted soil in post-peak regime outside shear band; (f) reconstituted soil in post-peak regime inside shear band

bo l , F ndacao a a a Ciencia e a Tecnologia, a of he PhD ea ch of he a ho . The a ho o ld al o like o e hei g a i de o GE Me emen & Con ol Sol ion (D eldo f, Ge man). The a ho g a ef l ackno ledge he EPSRC (EP/F001452/1 & EP/I02249X/1) fo f nding.

NOTATION

dA	inc emen al a ea
a , b , c	majo , in e media e and mino half leng h of a icle p
d_{50}	mean a icle i e
N	o al n mbe of ec o in em
N	n mbe of a icle
n_i^k	ni o ien a ion ec o along di ec ion i
p'	mean no mal effec i e (= ($\sigma_1 - \sigma_3$)/3)
q	de ia o ic (= $\sigma_1 - \sigma_3$)
$\boldsymbol{S}_{ij}^p$	ha e en o fo a icle p
$\boldsymbol{T}_{ij}$	o ien a ion en o fo a icle p
α	angle be een b anch ec o and con ac no mal
β	angle gi en b he majo inci al eigen ec o of fab ic en o
β^P	β fo he fab ic en o of he a icle long a i
ε_a	a ial ain
θ	o ien a ion of hea band

ν Poisson's ratio
σ_1 axial effective stress
σ_3 radial effective stress
Φ_{ij} fabric tensor
Φ_1, Φ_3 maximum and minimum eigenvalues of fabric tensor
Φ_{ij}^{a} fabric tensor that considers the shape and orientation of particles
$d\psi$ angular increment
ψ angle measured from the horizontal (x–y)
ω sum of all contact sizes
ω^k size of contact k

REFERENCES

Arthur, J. & Menzies, B. (1972). Inherent anisotropy in a sand. *Géotechnique* **22**, No. 1, 115–128, http://dx.doi.org/10.1680/geot.1972.22.1.115.

Atwood, R. C., Jones, J. R., Lee, P. D. & Hench, L. L. (2004). Analysis of pore interconnectivity in bioactive glass foams using X-ray microtomography. *Scripta Mater.* **51**, No. 11, 1029–1033.

Barreto, D. (2009). *Numerical and experimental investigation into the behaviour of granular materials under generalised stress states*. PhD thesis, University of London, UK.

Been, K. & Jefferies, M. G. (1985). A state parameter for sands. *Géotechnique* **35**, No. 2, 99–112, http://dx.doi.org/10.1680/geot.1985.35.2.99.

Beucher, S. & Lantuejoul, C. (1979). *Use of watersheds in contour detection*. Rennes, France: CCETT.

Cavarretta, I. (2009). *The influence of particle characteristics on the engineering behaviour of granular materials*. PhD thesis, Department of Civil and Environmental Engineering, Imperial College London, UK.

Chan, H. T. & Kenney, T. C. (1973). Laboratory investigation of permeability ratio of New Liskeard varved soil. *Can. Geotech. J.* **10**, No. 3, 453–472.

Cresswell, A. & Powrie, W. (2004). Triaxial tests on an unbonded locked sand. *Géotechnique* **54**, No. 2, 107–115, http://dx.doi.org/10.1680/geot.2004.54.2.107.

Cuccovillo, T. & Coop, M. R. (1999). On the mechanics of structured sands. *Géotechnique* **49**, No. 6, 741–760, http://dx.doi.org/10.1680/geot.1999.49.6.741.

Dafalias, Y., Papadimitriou, A. & Li, X. S. (2004). Sand plasticity model accounting for inherent fabric anisotropy. *J. Engng Mech.* **130**, No. 11, 1319–1333.

Tovey, N. K. & Dadey, K. A. (2002). Quantitative orientation and micro-porosity analysis of recent marine sediment microfabric. *Quaternary Int.* **92**, No. 1, 89–100.

Dusseault, M. B. & Morgenstern, N. R. (1979). Locked sands. *Q. J. Engng Geol.* **12**, No. 2, 117–131.

Fonseca, J. (2011). *The evolution of morphology and fabric of a sand during shearing*. PhD thesis, Imperial College London, University of London, UK.

Fonseca, J., O'Sullivan, C., Coop, M. R. & Lee, P. D. (2012). Non-invasive characterization of particle morphology of natural sands. *Soils Found.* **52**, No. 4, 712–722.

Haralick, R. & Shapiro, L. (1992). *Computer and robot vision*. Boston, MA, USA: Addison Wesley Longman.

Ibrahim, A. A. & Kagawa, T. (1991). Microscopic measurement of sand fabric from cyclic tests causing liquefaction. *Geotech. Test. J.* **14**, No. 4, 371–382.

Ibraim, E., Lanier, J., Muir Wood, D. & Viggiani, G. (2010). Strain path controlled shear tests on an analogue granular material. *Géotechnique* **60**, No. 7, 545–559, http://dx.doi.org/10.1680/geot.8.P.100.

Kuwano, R. & Jardine, R. J. (2002). On the applicability of cross-anisotropic elasticity to granular materials at very small strains. *Géotechnique* **52**, No. 10, 727–749, http://dx.doi.org/10.1680/geot.2002.52.10.727.

Mathworks (2011). MATLAB Release 7·12. Natick, MA, USA: Mathworks, Inc.

Ng, T.-T. (1999). Fabric study of granular materials after compaction. *J. Engng Mech.* **125**, No. 12, 1390–1394.

Ng, T.-T. (2004). Macro- and micro-behaviors of granular materials under different sample preparation methods and stress paths. *Int. J. Solids Struct.* **41**, No. 21, 5871–5884.

Oda, M. (1972). Initial fabrics and their relations to mechanical properties of granular material. *Soils Found.* **12**, No. 1, 17–36.

Oda, M. & Kazama, H. (1998). Microstructure of shear bands and its relation to the mechanisms of dilatancy and failure of dense granular soils. *Géotechnique* **48**, No. 4, 465–481, http://dx.doi.org/10.1680/geot.1998.48.4.465.

Oda, M., Nemat-Nasser, S. & Konishi, J. (1985). Stress induced anisotropy in granular masses. *Soils Found.* **25**, No. 3, 85–97.

O'Sullivan, C. (2011). *Particulate discrete element modelling*. London, UK: Taylor & Francis.

Phillion, A. B., Lee, P. D., Maire, E. & Cockcroft, S. L. (2008). Quantitative assessment of deformation-induced damage in a semisolid aluminum alloy via X-ray microtomography. *Metall. Mater. Trans. A* **39**, No. 10, 2459–2469.

Satake, M. (1982). Fabric tensor in granular materials. *Proceedings of the IUTAM conference on deformation and failure of granular materials*, Delft, pp. 63–67.

Shire, T., O'Sullivan, C., Barreto, D. & Gaudray, G. (2012). Quantifying stress-induced anisotropy using inter-void constrictions. *Géotechnique*, http://dx.doi.org/10.1680/geot.11.T.020.

Thornton, C. (2000). Numerical simulations of deviatoric shear deformation of granular media. *Géotechnique* **50**, No. 1, 43–53, http://dx.doi.org/10.1680/geot.2000.50.1.43.

Vaid, Y. P. & Sivathayalan, S. (2000). Fundamental factors affecting liquefaction susceptibility of sands. *Can. Geotech. J.* **37**, No. 3, 592–606.

Ventouras, K. & Coop, M. R. (2009). On the behaviour of Thanet Sand: an example of an uncemented natural sand. *Géotechnique* **59**, No. 9, 727–738, http://dx.doi.org/10.1680/geot.7.00061.

Wilkinson, S. (2011). *The microstructure of UK mudrocks*. PhD thesis, Imperial College London, University of London, UK.

Zdravkovic, L. & Jardine, R. (1997). Some anisotropic stiffness characteristics of a silt under general stress conditions. *Géotechnique* **47**, No. 3, 407–438, http://dx.doi.org/10.1680/geot.1997.47.3.407.

Zhang, Q., Lee, P. D., Singh, R., Wu, G. & Lindley, T. C. (2009). Micro-CT characterization of structural features and deformation behavior of fly ash/aluminum syntactic foam. *Acta Mater.* **57**, No. 10, 3003–3011.